PNAS Template for Supporting Information

This PNAS template for Supporting Information (SI) may be used to organize your supporting material. **Once formatted, this first page should be deleted by removing the `\instructionspage` command.** The template is intended to provide a clearly organized PDF file that will ensure readers can easily navigate to sections or specific figures and tables. Movie files or large datasets can be presented as separate files. Further information is available in the PNAS Author Center.

Using the template

Specify the title, author list, and corresponding authors with the `\title`, `\author` and `\correspondingauthor` commands. The cover page will be automatically generated with the relevant description of the SI, by the `\maketitle` command.

Figures should be placed on separate pages with legends set immediately below each figure. Table titles should be set immediately above each table. Note that tables extending beyond the width of the page can be included in the PDF or provided as separate dataset files. Oversized/nonstandard page sizes are accepted as part of your SI Appendix file.

References cited in the SI text should be included in a separate reference list at the end of this SI file: (**?**) and (**?**).

Supporting information for Brief Reports is limited to extended methods, essential supporting datasets, and videos (no additional tables or figures). Supporting figures and tables are not allowed for Brief Reports.

Submitting SI

Delete this first page by removing the `\instructionspage` command, and then save your completed SI file as a PDF for submission. Further submission instructions are available here.

Supporting Information for

Supporting Information for Dynamic Gardner crossover in a simple glass

Qinyi Liao, Ludovic Berthier, Hai-Jun Zhou and Ning Xu

Qinyi Liao.
E-mail: qinyi.liao.phy@gmail.com
Ludovic Berthier.
E-mail: ludovic.berthier@umontpellier.fr
Hai-Jun Zhou.
E-mail: zhouhj@itp.ac.cn
Ning Xu.
E-mail:ningxu@ustc.edu.cn

This PDF file includes:

Supporting Information Text

State-following analysis for ultrastable glasses. We compare the results using the state-following protocol used in earlier work to the results in the main text for ultrastable glass states. Specifically the state-following protocol is used from the equilibrium states of $\varphi_g = 0.860$, and it is compared to the ultrastable states prepared at $(\varphi_g = 0.860, Z_s = 200, t_s = 2^{18} \times 100)$ used in the main text. As shown in Fig. S1, the two protocols give consistent results. In both cases, the long-time limits of cage-relative MSD Δ and mean-squared clone distances $\langle \Delta_{ab} \rangle$ are roughly equal when $Z < Z_G \approx 10^3$ and deviate from one another upon increasing the pressure further.

Therefore, the Gardner crossover using the protocols of ultrastable glass samples agrees well with the result obtained by the state-following protocol for corresponding metastable equilibrium glasses.

Complex dynamics at high pressures. To better characterise the crossover to the complex dynamics in arbitrary protocols, we compute the evolution of the probability for the clone distance to be smaller than the typical cage size,

$$F(\Delta_{ab} \leq \langle \Delta \rangle) = \int_0^{\langle \Delta \rangle} d\Delta_{ab} \; P(\Delta_{ab}). \qquad [1]$$

Here the mean-squared cage size $\langle \Delta \rangle$ can be measured from the plateau value of $\Delta(t_w, t)$, and it captures the averaged size of the basins at a given Z condition, and $P(\Delta_{ab})$ is the probability distribution function of clone mean-squared distances. For simple glasses in the absence of aging relaxation, $P(\Delta_{ab})$ is approximately Gaussian with the mean value $\Delta_{ab} \approx \langle \Delta \rangle$, corresponding to $F \approx 0.5$, as shown by the results for ultrastable glasses at $Z = 200$ and $Z = 600$ in Fig. S2(c). On the other hand, if the dynamics is dominated by aging diffusion dynamics, most of the clones jump out of the initial basin and explore different portions of the landscape. As a result, $F(t_w)$ decreases to a smaller value as more clone distances become larger. This occurs when following ordinary and marginal glasses at relatively low pressures, see Figs. S2(a, b). Upon compression, all three glasses to high enough pressures, the dynamics becomes slow, accompanying the emergence of a complex landscape, leading to the overall decrease of $F(t_w)$, as shown in Fig. S2. Meanwhile, as some clones cross some barriers and fall into the same more stable sub-basins, $F(t_w)$ grows for a long time. As shown by the results at high pressures in Fig. S2, the clone dynamics of ordinary glasses and marginal glasses is analogous to the case of ultrastable glasses, and can thus be used to determine a dynamic Gardner crossover.

Robustness of Gardner physics. We study the dynamic Gardner crossover by compressing the ordinary glasses produced at shorter t_s. As an example, we show the result of the glass prepared using the parameters of $\varphi_g = 0.600, Z_s = 100$ and $t_s = 2^{10} \times 100$. As shown in the main text, the dynamics of representative glass exhibits strong structural relaxations, and the plateau of the MSD $\Delta(t)$ is nearly observed indicating the formation of transient cages. We employ these highly unstable glasses as our samples and compress them at various pressures as in the main text. In Fig. S3(a), we plot the evolution of the probability distribution of mean-squared clone distances $P(\Delta_{ab})$ at $Z = 400$, from which one can see that $P(\Delta_{ab})$ develop a peak centered at $\langle \Delta \rangle$ with time. It suggests a dynamic Gardner crossover for this protocol. We then compute the cumulative probability $F(t_w)$ to determine threshold pressure. As shown by Fig. S3, when increasing Z larger than $Z_G \approx 200$, $F(t_w)$ turns to increase over time which is qualitatively similar to the results of more stable glasses in Fig. S2. We thus conclude that Gardner physics is considerably robust against structural relaxation in hard disk glasses.

Evidence for hierarchical dynamics. In this section, we analyze the correspondence between sampling the glass landscape and aging dynamics for ordinary glasses by focusing on individual samples. We study representative samples prepared from compressing independent configurations at $\phi_g = 0.600$ to $Z_s = 100$ for $t_s = 2^{18} \times 100$, using $N_c = 100$ clones for each sample. The dynamic Gardner crossover for such ordinary glasses is estimated at $Z_G \approx 300$. For the system size $N = 1024$, we observe strong sample-to-sample fluctuations. The aging behaviors are roughly classified into three categories within the time window $\sim 3 \times 10^7$, as illustrated in Fig. S4. The overall amplitude of the aging dynamics varies from one sample to another, corresponding to distinct evolution of the distribution of clone displacement $P(\Delta_{ab})$.

To better reveal the hierarchical structure of the landscape, we indicate the three characteristic mean-squared cage sizes $\langle \Delta \rangle$ for the protocols at $Z = Z_s = 100$, $Z = Z_G = 300$, and $Z = 800$. As seen in Fig. S4(d), $P(\Delta_{ab})$ for the first sample develops a bimodal structure with increasing t_w, with two peaks centered at $\langle \Delta \rangle(Z = 800)$ and $\langle \Delta \rangle(Z = 300)$. This suggests the emergency of smaller clusters of clones, where the typical distance between within each cluster is $\langle \Delta \rangle(Z = 800)$, while the average distance between clusters is $\langle \Delta \rangle(Z = 300)$.

As shown in the main text, $P(\Delta_{ab})$ for the second sample develops a tail up to $\langle \Delta \rangle(Z = 100)$, meaning that the whole basin selected by the initial state at $Z_s = 100$ remains dynamically accessible. Correspondingly, this sample shows stronger aging dynamics, compare to Figs. S4(a, b).

The third sample, shown in Figs. S4(c, f) exhibits the strongest aging dynamics among the three cases, and the clone distances can significantly exceed $\langle \Delta \rangle(Z = 10^2)$, implying the existence of structural relaxation beyond the initial basin. Note that this classification is empirical since the simulation duration is limited. When t_w is long enough, all samples should resemble the third example. Nevertheless, there are growing peaks at the small distances near $\langle \Delta \rangle(Z = 800)$ at long times in all cases, indicating that some clones remain close to one another, which is indicative of Gardner physics.

We next visualise the topological structure of the landscape detected by the clones for the three samples at $Z = 800$. We plot the heat maps of clone distances Δ_{ab} for the states in Fig. S4 in Fig. S5. The choice of clone ordering is irrelevant to the

structure of the data and is only useful for illustrative purposes. The current choice is based the clustering order. In the first sample, two major clusters form at intermediate time scales, and one of them shrinks at longer t_w as clones eventually end in the more stable sub-basin. This is similar to the situation seen when compressing the ultrastable glasses at $Z > Z_G$.

By contrast, the situation for the second and third samples is more complicated, since the time scales of aging events in different glass basins are close. The heatmap reveals the presence of independent basins (explored via aging relaxation) in which a hierarchical Gardner structure emerges, see Figs. S5(b, c). These hierarchical heat maps reveal the intricate structure underlying the broad distributions in Figs. S4(e, f).

Susceptibility analysis for stable states. We consider the glass states prepared by compressing the equilibrium glasses of $\varphi_g = 0.820 > \varphi_{MCT} \approx 0.795$ at $t_s = 2^{18} \times 100$ and different $Z_s = 10^5$, 10^4, 10^3, 300 and 10^2. The Gardner crossover is found to occur near $Z_G(\varphi_g = 0.820) \approx 200$ when using the standard state-following scheme. Thus, the glasses produced at $Z_s \geq 200$ are marginally stable.

When we make clones at the pressure of $Z = Z_s$, as in the main text, the corresponding susceptibility has the behaviour shown in Fig. S6(c). For $Z = 10^2 < Z_G$, $\chi_{AB}(t_w)$ reaches a small value $\chi^*_{AB} \sim 3$ after a time scale $t_w \sim 10^4$. By contrast, the susceptibility for marginal glasses of $Z \geq Z_G$ grows over the entire time window, owing to the slow dynamics in the presence of small barriers. We conclude that the susceptibility analysis presented in the main text provides results consistent with the state-following analysis used in previous studies when the latter can be used. In Fig. S6(a), we report the long-time distributions $P(\Delta_{ab})$ for the same data. In line with the behavior of χ_{AB}, $P(\Delta_{ab})$ is Gaussian at $Z = 10^2$. Upon compressing to $Z \geq Z_G$, there are activated events in the Gardner region. As a result, $P(\Delta_{ab})$ extends to larger Δ_{ab} with respect to the Gaussian distributions of short time vibrations. We also display the organization of the clones for $(Z = 10^3, t_w = 2^{18} \times 100)$ for a representative sample of $(Z_s = 10^3)$ in Fig. S6(b).

In summary, the analysis of marginal glasses following the analysis proposed in the main text leads to qualitatively similar findings as for ordinary glasses, even though the structural relaxation is highly suppressed for the marginal states.

Susceptibilities upon approaching jamming. In the main text, we show that the susceptibility χ_{AB} extracted from the evolution of ordinary glasses at $Z = Z_s$ grows with increasing pressure. Here we report the dependence of $\chi_{AB}(t_w)$ on the density for ordinary glasses prepared at fixed $(\varphi_g = 0.600, Z_s = 10^2)$. When rapidly compressing these fluid states to $Z_s > Z_{MCT}$, the system falls out of equilibrium and undergoes evident densification at long times. Hence t_s controls the density of ordinary glasses. In Fig. S7, we show the evolution of $\chi_{AB}(t_w)$ for the initial states generated at $t_s = 0 - 2^{21} \times 100$. One can see that $\chi_{AB}(t_w)$ takes small values for short t_s. With increasing the time t_s, the stability, and density increase, the structural relaxations are less pronounced, and the long-time susceptibility becomes larger.

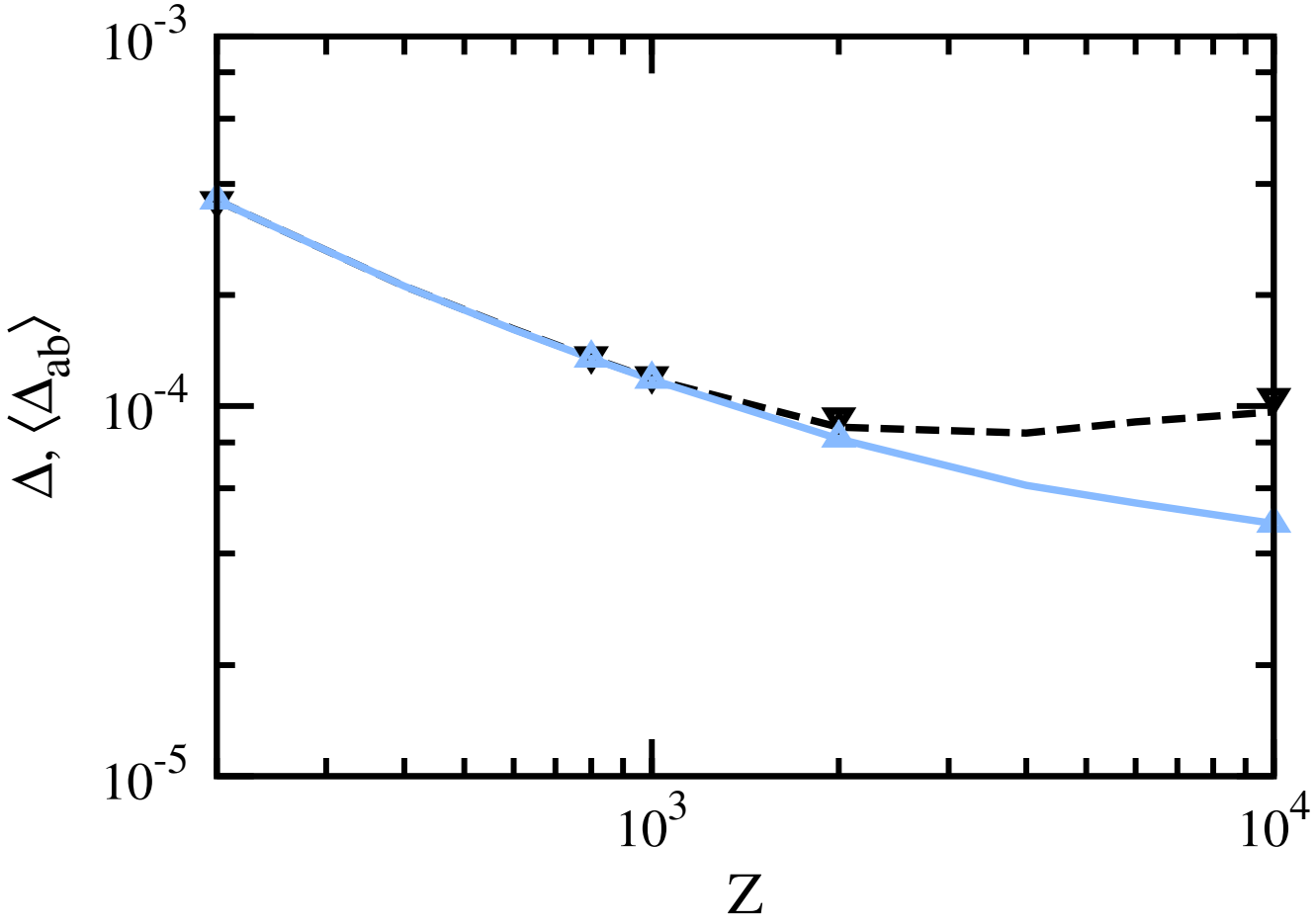

Fig. S1. The long-time cage-relative MSD Δ for $t_w = t = 2^{17} \times 100$ (blue) and the cage-relative mean-squared clone distances $\langle\Delta_{ab}\rangle(t_w = 2^{17} \times 100)$ (black) as a function of pressure. The points are measured from the protocols described in the main for ultrastable glasses with $(\varphi_g = 0.860, Z_s = 200, t_s = 2^{18} \times 100)$, and the lines are the corresponding data for state-following equilibrium glasses with $\varphi_g = 0.860$.

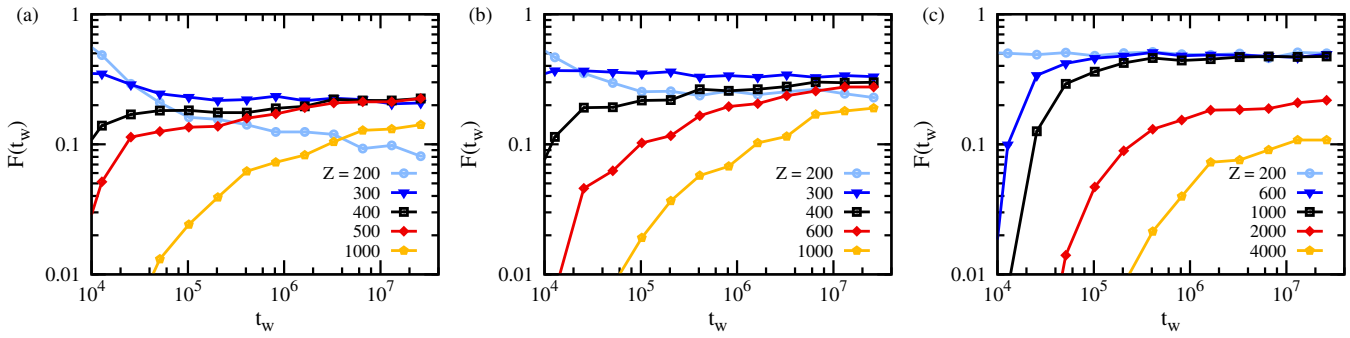

Fig. S2. Probability that the clone distance is smaller than the mean-squared cage size as the function of waiting time. The protocols are the same as in the main text where the systems are prepared by compressing equilibrium states at $\varphi_g = 0.600$ in (a), 0.820 in (b) and 0.860 in (c) to $Z_s = 200$ for a time $t_s = 2^{18} \times 100)$, resulting in ordinary, marginal and ultrastable glasses. In all cases, F increases with t_w at high enough pressures, corresponding to falling into sub-basins. The crossovers to these dynamics are estimated at $Z_G \approx 500, 400$, and 10^3.

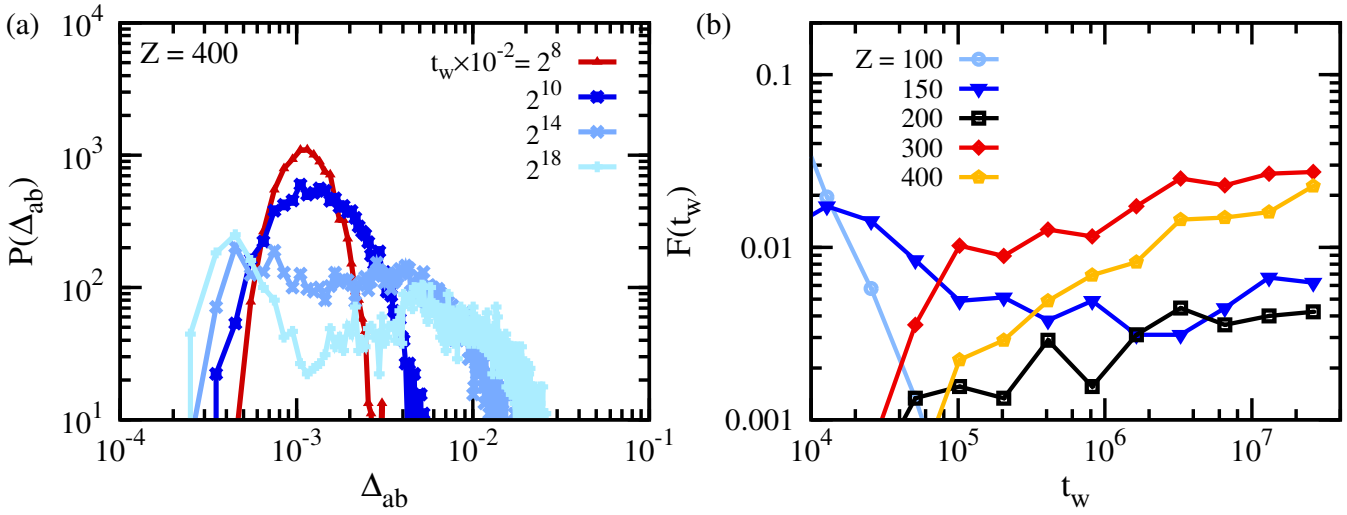

Fig. S3. (a) Evolution of the distributions of mean-squared cage-relative distances between clones $P(\Delta_{ab})$ at $Z = 400$ for the less stable samples compressed from the equilibrium states of $\phi_g = 0.600$ on the condition of $(Z_s = 10^2, t_s = 2^{10} \times 100)$ shown in the main text. (b) The cumulative probability for the clone distance being smaller than the cage size as the function of waiting time. The states are respectively generated at $Z = 100, 150, 200, 300$ and 400 using the samples. The crossover is estimated at $Z_G \approx 200$.

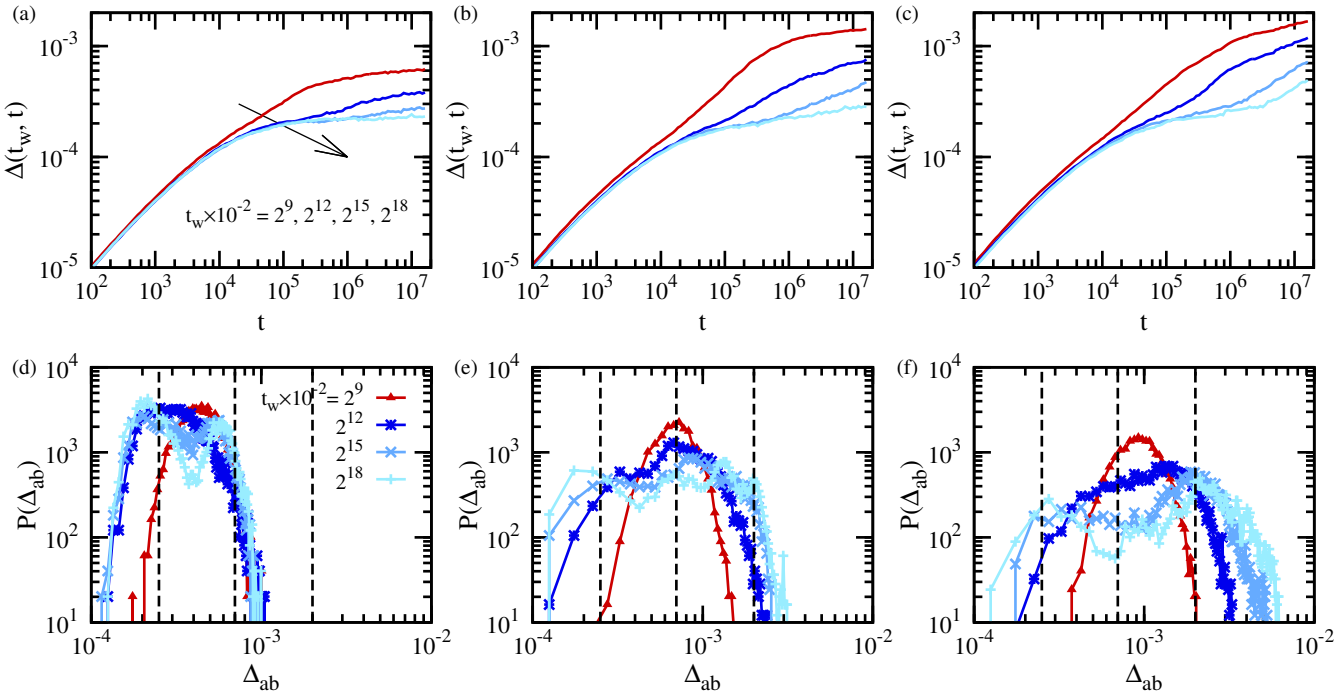

Fig. S4. (a-c) The cage-relative MSDs $\Delta(t_w, t)$s for the protocols of following three individual ordinary glass samples of $(\varphi_g = 0.600, Z_s = 100, t_s = 2^{18} \times 100)$ at a intermediate pressure higher than the crossover pressure $Z = 800 > Z_G \approx 300$. $N_c = 100$ clones are used for each of the three samples. (d-f) The related probability distributions of clone displacement $P(\Delta_{ab})$s. Here the results shown in the same column correspond to the same protocol. The values of mean-squared cage sizes $\Delta_{EA}(Z = 800) \approx 2.5 \times 10^{-4}$, $\Delta_{EA}(Z = 300) \approx 7 \times 10^{-4}$ and $\Delta_{EA}(Z = 100) \approx 2 \times 10^{-3}$ are denoted with the vertical dashed lines.

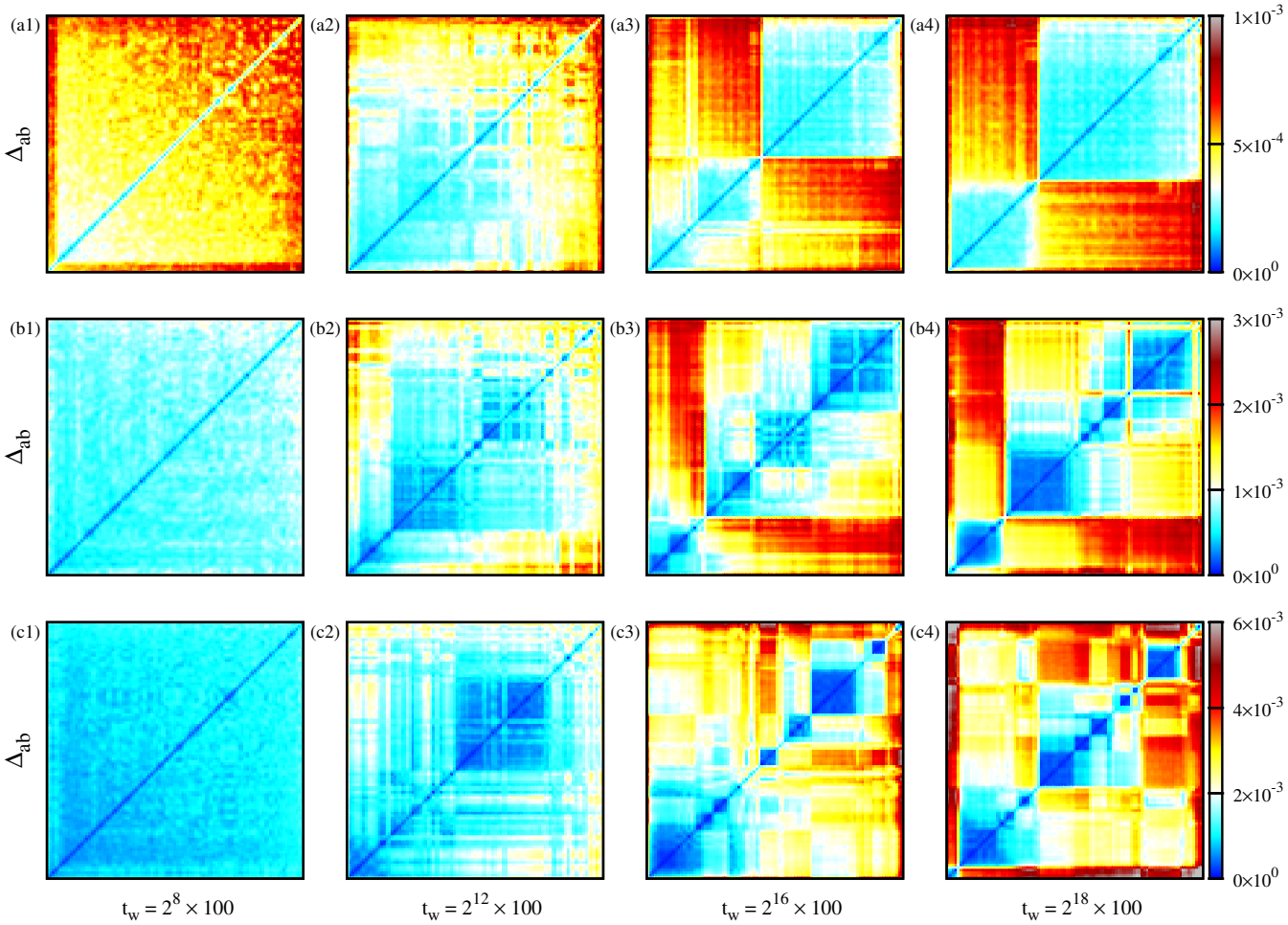

Fig. S5. Heat maps constructed with $N_c = 100$ clones for Δ_{ab} between clones copied from different ordinary glass samples taken at $(\varphi_g = 0.600, Z_s = 10^2, t_s = 2^{18} \times 100)$ are shown in different rows. Here the following pressure is $Z = 800$ as in Fig. S4. For each column, the waiting time after crunches is fixed and varies from $2^8 \times 100$ to $2^{18} \times 100$ as indicated by labels. For each sub-graph, the axes and the color represent the clone indexes and Δ_{ab} respectively.

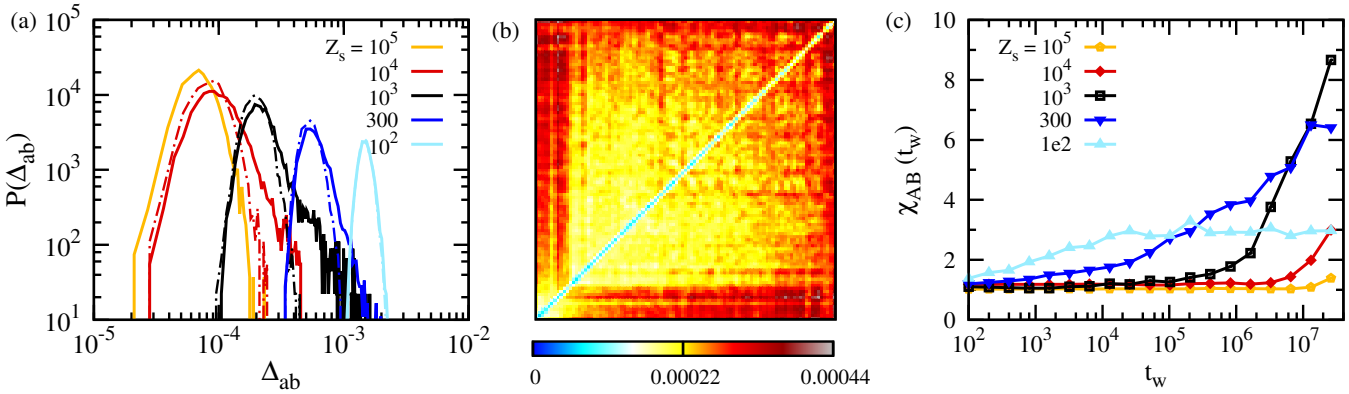

Fig. S6. (a) Probability distributions of mean-squared clone distances $P(\Delta_{ab})$ for the protocol of various $Z = Z_s$ using $t_s = 2^{18} \times 100$ and $(N_s = 100, N_c = 10)$ at $t_w = 2^{18} \times 100$. From left to right, the pressures are $Z = Z_s = 10^5, 10^4, 10^3, 300$ and 10^2. The short-time vibration behaviors are conveyed by dotted curves acting as references. At $Z_s = 10^5$, $t_w = 2^{18} \times 100$ is not long enough to form the well-defined cages. We thus are not able to present the Gaussian-like reference for $Z_s = 10^5$. (b) Heat map for a representative sample with $(\varphi_g = 0.820, Z_s = 10^3, t_s = 2^{18} \times 100)$ at $Z = Z_s$ and $t_w = 2^{18} \times 100$. (c) Evolution of the corresponding susceptibility $\chi_{AB}(t_w)$ for the same protocols in (a).

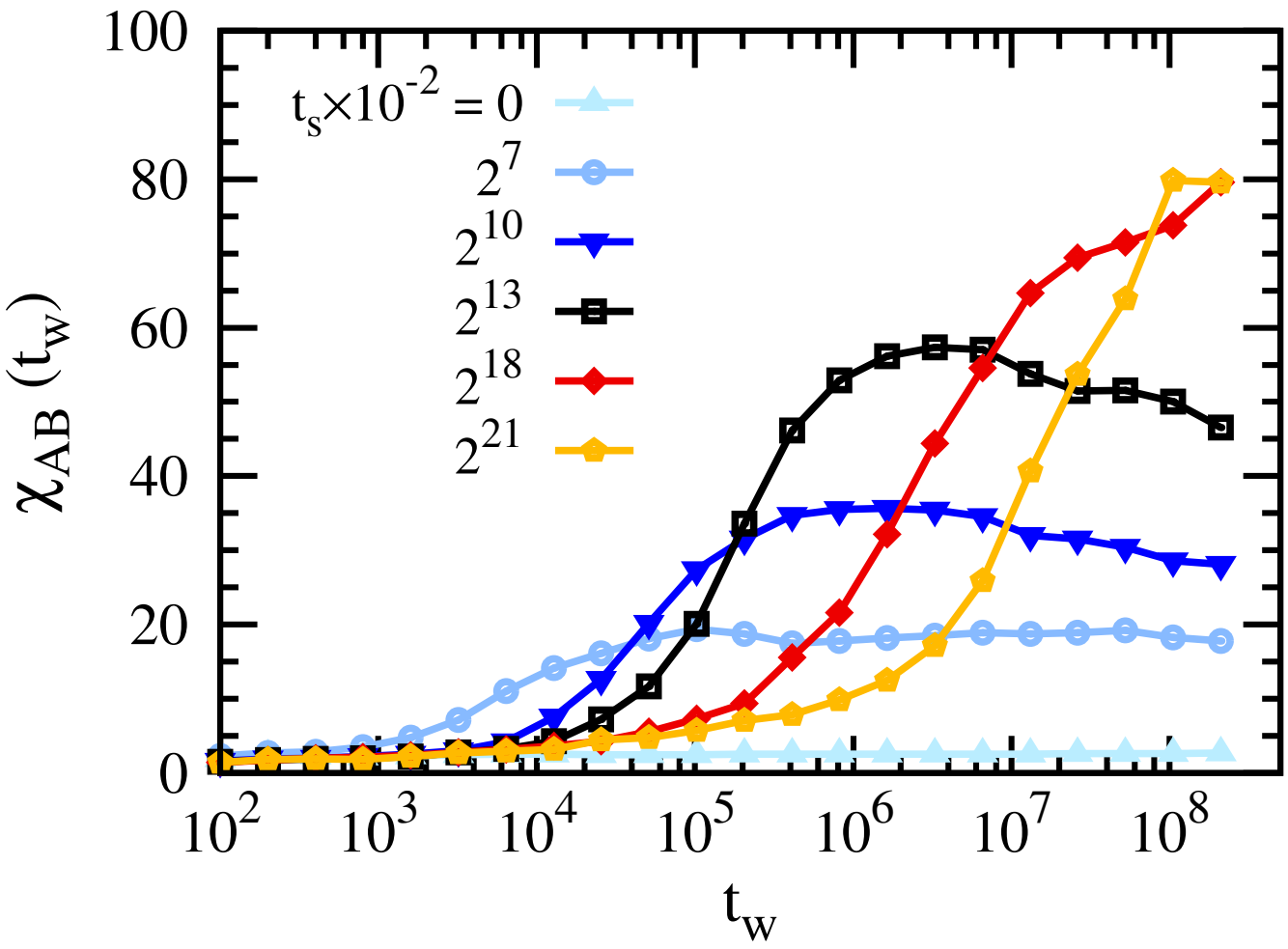

Fig. S7. Evolution of susceptibility $\chi_{AB}(t_w)$ for $(\varphi_g = 0.600, Z = Z_s = 10^2)$ at different preparation times t_s. The corresponding packing fractions are $\varphi_s \approx 0.8081, 0.8320, 0.8346, 0.8355$ and 0.8361 at $t_s = 2^7 \times 100, 2^{10} \times 100, 2^{13} \times 100, 2^{18} \times 100$ and $2^{21} \times 100$ respectively. With the densification at longer t_s, ordinary glasses become more stable and show larger χ^*_{AB}.